Analysis of Low-Dimensional Radio-Frequency Impedance-Based Cardio-Synchronous Waveforms for Biometric Authentication

Shreyas Venugopalan*, *Student Member, IEEE*, Marios Savvides, *Member, IEEE*, Marc O Griofa, and Ken Cohen

***Abstract*—Over the past two decades, there have been a lot of advances in the field of pattern analyses for biomedical signals, which have helped in both medical diagnoses and in furthering our understanding of the human body. A relatively recent area of interest is the utility of biomedical signals in the field of biometrics, i.e., for user identification. Seminal work in this domain has already been done using electrocardiograph (ECG) signals. In this paper, we discuss our ongoing work in using a relatively recent modality of biomedical signals—a cardio-synchronous waveform measured using a Radio-Frequency Impedance-Interrogation (RFII) device for the purpose of user identification. Compared to an ECG setup, this device is noninvasive and measurements can be obtained easily and quickly. Here, we discuss the feasibility of reducing the dimensions of these signals by projecting onto various subspaces while still preserving interuser discriminating information. We compare the classification performance using classical dimensionality reduction methods such as principal component analysis (PCA), independent component analysis (ICA), random projections, with more recent techniques such as K-SVD-based dictionary learning. We also report the reconstruction accuracies in these subspaces. Our results show that the dimensionality of the measured signals can be reduced by 60 fold while maintaining high user identification rates.**

***Index Terms*—Biometrics (access control), biomedical equipment, biomedical signal processing, electrocardiography, pattern matching, pattern recognition.**

I. Introduction

THE application of signal processing techniques in the biomedical field has taken great strides in the past few years due to significant advances in measuring devices and instrumentation. Magnetic resonance imaging (MRI), positron emission tomography, electroencephalography (EEG), and electrocardiogram (ECG) are examples of signal modalities that aid in performing relevant diagnoses and in studying various biological mechanisms in the human body. ECG signals have recently been studied in a user identification context. Recent works such as those by Li and Narayanan [18], Plataniotis *et al.* [19], and Singh and Singh [22] discuss the previous literature and suggest improvements to the same in order to improve the recognition performance using this signal modality. Albeit, an easily accessible modality, acquiring a subject's ECG signal requires contact electrodes to be attached to the subject. This may not be desirable or even feasible in certain situations. For example, receiving cardio-synchronous signals from warfighters during combat, is a desirable application from both a medical perspective as well as from the perspective of imposter detection (e.g., an enemy in uniform, impersonating a friendly). It is neither possible nor desirable to have contact or "invasive" methods of signal acquisition in this scenario. In this paper, we describe our work in using a novel, noncontact device to acquire a cardio-synchronous waveform from a subject and we explore a few methods on how these signals may be used for user identification. By noncontact in this paper, we mean that the device does not require the use of electrodes attached to the subject's skin for data collection. It merely has to be placed over the chest, over clothing, when being used.

Noninvasive medical technologies (NMT) has recently developed this radio frequency impedence interrogation (RFII) device capable of acquiring cardio-synchronous signals from a user's thoracic cavity. A brief description of the device can be found in the work by Griofa *et al.* [12]. We provide a more detailed overview in Section II. A 5 s snippet of a recording from this device is shown in Fig. 1(b). This is the output from the device as measured in millivolts (mV). Fig. 1(c) and (d) shows the extracted information during one cardiac cycle in the recording. These "beats" from the recording are normalized to have zero mean and unit variance in this study. In order to extract the individual "beats," the wavelet-based segmentation approach proposed by Bhagavatula *et al.* in [5] is used. The corresponding ECG recording during the same interval is shown in Fig. 1(a), in order to show the cardio-synchronous nature of the RFII signal. All segmented "beats" used in this study are of this normalized type unless otherwise mentioned.

Some preliminary work has been done, using signals acquired from this device, for user identification. A pilot study on the utility of these signals for biometrics can be found in the work by Griofa *et al.* in [13]. Jaech *et al.* in [16] have modeled the signal using the Legendre polynomials in order to compare signals from various users. They used a small dataset and were able to experimentally verify the existence of user specific features

Manuscript received October 23, 2012; revised March 7, 2013 and May 22, 2013; accepted June 19, 2013. Date of publication July 3, 2013; date of current version July 15, 2014. *Asterisk indicates corresponding author.*

*S. Venugopalan is with the CyLab Biometrics Center and the Department of Electrical and Computer Engineering, Carnegie Mellon University, Pittsburgh, PA 15213 USA (e-mail: svenugop@andrew.cmu.edu).

M. Savvides is with the CyLab Biometrics Center and the Department of Electrical and Computer Engineering, Carnegie Mellon University, Pittsburgh, PA 15213 USA (e-mail: msavvid@ri.cmu.edu).

M. O Griofa is with the Noninvasive Medical Technologies, Las Vegas, NV 89118 USA (e-mail: mogriofa@nmtinc.org).

K. Cohen is with the Physiology and Engineering Research lab, InoMedic Health Application, Inc., Merritt Island, FL 32953 USA (e-mail: kcohen@ihamedical.com).

Color versions of one or more of the figures in this paper are available online at http://ieeexplore.ieee.org.

Digital Object Identifier 10.1109/TBME.2013.2272038

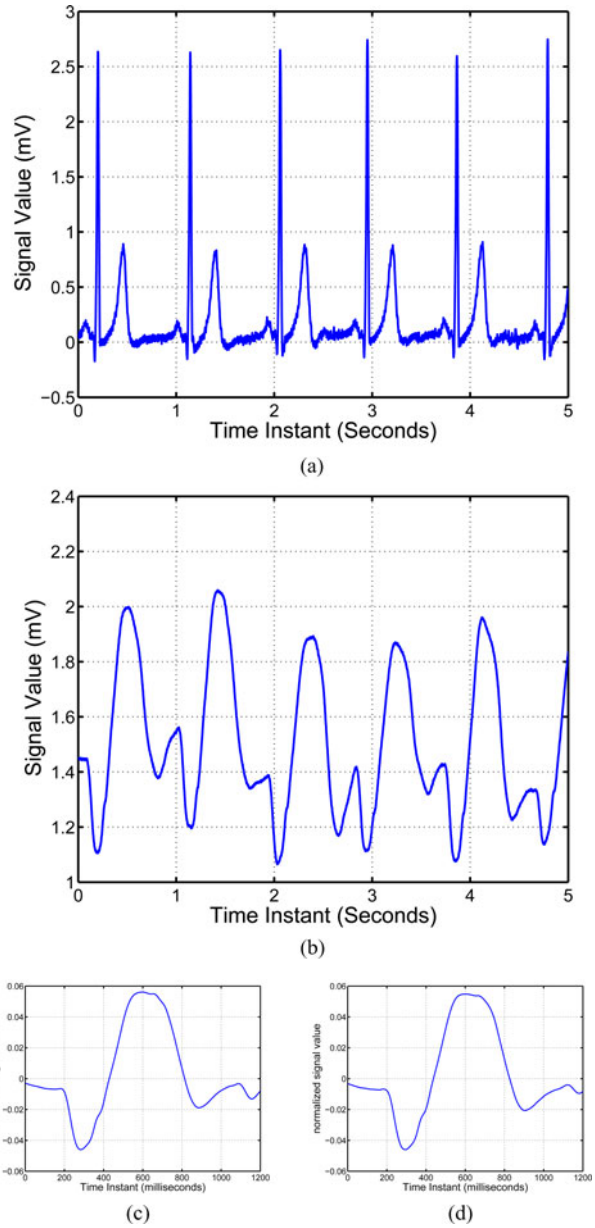

Fig. 1. (a) Five seconds of the ECG recording of a subject captured along with the RFII output signal (b) corresponding recording made using the RFII device, measured in milli Volts (mV). (c) and (d) shows examples of "beats" from the recording in (b), i.e., segments corresponding to a cardiac cycle. After extracting all beats from a recording, they are normalized to have zero mean and unit variance.

using these polynomails, due to which high user identification rates are obtained. Wavelet-based feature extraction using these signals and the corresponding verification rates were reported in the work by Bhagavatula *et al.* in [4]. The utility of using correlation filters to extract relevant features from these signals is discussed in [6].

The purpose of this paper is to demonstrate the performance of some of the common subspace modeling techniques on this data and to report the results for a set of user identification experiments. In addition, we report the genuine and imposter match scores which are useful when this modality is used in

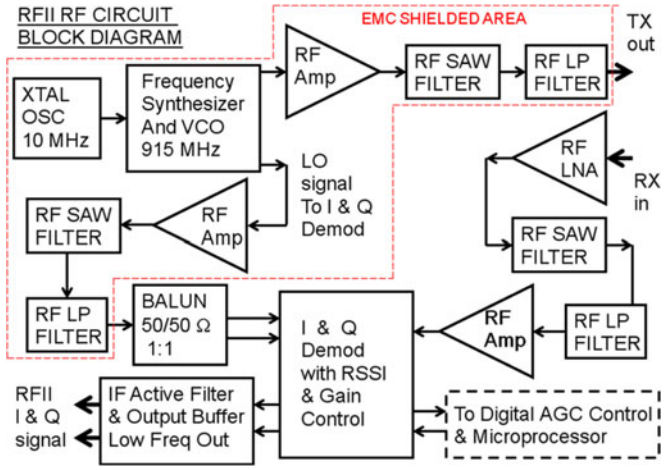

Fig. 2. RFII device block diagram.

a user verification context. The classifier used uses a standard nearest neighbor approach within the subspaces built. We also use support vector machine (SVM) models in some of the experiments and compare the performance of both these classifiers. In addition to user identification experiments, the reconstruction accuracy of the original high dimensional signal from a low dimensional representation in these subspaces is also investigated. The classical methods we have worked on for this article include principal component analysis (PCA), independent component analysis (ICA), and the random projection (RP) method. These techniques utilize coefficients determined by the projection of data samples on the estimated bases. In addition, we also built an overcomplete dictionary for discriminative sparse representation of data samples. The approach used for this is the K-SVD algorithm that was proposed by Aharon *et al.* in [1]. For this set of experiments, we reconstructed the original signal from a sparse coefficient set and used the reconstructed signals for identification. Further details are given in the later half of this paper. We provide details about the RFII device used, in Section II. Section III briefly describes the theory behind these subspace modeling techniques. Experiments and comparison of identification rates obtained using these methods are presented in Section IV. A few concluding remarks and directions for future work are given in Section V.

II. Description of the RFII Device

In this section, we provide a description of the RFII device used in our study. A block diagram of the device is shown in Fig. 2. It can be described in terms of three basic functional components:

1) *Radio Frequency Transmitter/Receiver Unit:* The device works on the principle of electromagnetic near-field resonant coupling, where the coupling to body tissue is due to the water dominated dielectrics, packaged with polar and nonpolar molecules [20]. It utilizes a commercial RF integrated circuit which incorporates a frequency synthesizer and voltage-controlled oscillator (VCO). The

frequency synthesizer is programmed to work in the 915 industrial-scientific-medical (ISM) frequency band, at frequency settings from 905 to 925 MHz. The frequency synthesizer-VCO is a true phase-lock-loop source, which has its frequency fixed by a 10 MHz crystal oscillator and has dual phase locked outputs with excellent frequency and RF power stability. Both transmit (TX) and local oscillator signals have fixed RF frequency and amplitude levels.

2) *Transducer-Antenna-Probe (TAP):* The TAP is a bidirectional component like an antenna. It is based on a modified quarter-wave microstrip antenna design. Unlike a conventional antenna, designed to radiate and receive RF power in free space, the TAP design is modified to couple the TX signal efficiently with the human thorax. It has a kite shape geometry and uses a high dielectric constant material. This ensures maximal coupling and has enough directionality to confine the energy to the cardiac tissue mass.
3) *High Isolation Full Duplexer (HIFD):* The HIFD isolates the received resonant signal (RX) from the TX signal. The RX signal is modulated in phase by cardiac motion and volume changes. The modulation is pronounced in high dielectric constant materials, like muscle and blood tissues. Since the received resonant signal is lower in power than the transmitted signal, the HIFD provides an isolation of more than -30 dB, in order to keep the TX signal out of the receiver channel.

The optimum position to place the TAP during signal acquisition is at the surface of the lower sternum. This position aids in coupling the RF energy to the heart. The breastbone has a significantly lower dielectric constant (10.0) than the heart—51.0 for muscle and 60.0 for blood (see [21]). Due to this as well as low signal loss in the bone, the RF energy can reach the heart with minimal loss at this position, than if it had to penetrate solid muscle. All measurements made for the purpose of experiments in this paper, are made at the lower sternum.

The RFII system transmits a single unmodulated RF tone set between 905 to 925 MHz. The TAP directs the transmitter tone to the blood and tissue of the cardiac mass below the sternum. It couples the RFII transmitter tone energy to the cardiac tissue, which has a dipole relaxation property similar to pure water dipole relaxation. The time constant for dipolar relaxation in water ranges from microseconds for large globular proteins to picoseconds for smaller molecules [2]. The RFII transmitter energy is at a good frequency range for RF resonant coupling with dipoles present in the cardiac tissue [21]. At or near resonant frequencies, changes in blood volume and cardiac motion, during the cardiac cycle, will create small deviations in the resonant coupling frequency, introducing a significant phase shift in the reflected signal [9]. As a result of this, a cardio-synchronous waveform is generated at the the RFII device's I and Q demodulated channel outputs, with significant information at very low frequencies (from a few hundred hertz to less than 100 millihertz)—see Fig. 2. We use the I-channel output in our experiments for the purpose of this paper.

III. Overview of Modeling Techniques Used

In this section, we describe the various data driven and nondata-driven modeling approaches used in this paper. We will first very briefly outline two well-documented methods—PCA and ICA. Following this, we will describe the RP method and how we use it in conjunction with the K-SVD-based dictionary building method in order to solve a user identification problem using the RFII signals.

A. Principal Component Analysis

PCA when applied to a given dataset, determines the directions of maximum variance in the data. These directions, the principal components (PCs) are determined by computing the covariance matrix Σ followed by its eigen decomposition which will give us the principal components (the eigen vectors of Σ) $\{\mathbf{v_i}|i = 1, 2, \ldots, D\}$. By projecting the data onto the PCs, we obtain a set of coefficients for each data sample, which are used as features for classification.

In our study, in order to generate the PCA subspace, the individual beats extracted from the recordings are used. As mentioned later in Section IV, our dataset is divided into a training and a testing set. The PCA subspace is built using all the beats extracted from the recordings in the training set (after normalizing them to have zero mean and unit variance, as mentioned earlier). The covariance matrix Σ is determined using these normalized beats, after which eigen decomposition gives us the principal components. A few examples of PCs obtained from PCA analysis of our dataset are shown in Fig. 3. In Fig. 4, we show signal reconstruction using different numbers of bases -5, 10, and 20. As will be seen from the later sections, projection onto the PCA subspace shows lesser reconstruction error as compared to other methods described in this paper. This error is calculated as the average mean squared error across the entire database, between the reconstructed signal and the original signal. Table I reports the signal reconstruction errors.

B. Independent Component Analysis

ICA is a popular technique employed in the field of biomedical signal processing, used when there is a need to separate multichannel biomedical signals into their constituent underlying components. It is essentially a technique to extract a set of underlying sources from a set of observed multivariate data in order to build a generative model for the observed data. In our study, the individual components are assumed to be mixed linearly and the mixing model is assumed to be unknown. Within the context of the RFII measurements, the observed data are taken to be multiple heartbeat samples from a single recording [such as one shown in Fig. 1(b)]. Our viewpoint in this experiment is that there are a finite number of overlapping activites(components) which are being measured by the RFII device during every heartbeat duration [refer to Fig. 1(c) and (d)] for an example of an RFII signal within a heartbeat duration). Assuming there are K unknown sources that contribute to the RFII measurement during every heart beat cycle. In that case, a vector of observations $\mathbf{x_i}$ at a given time instant can be

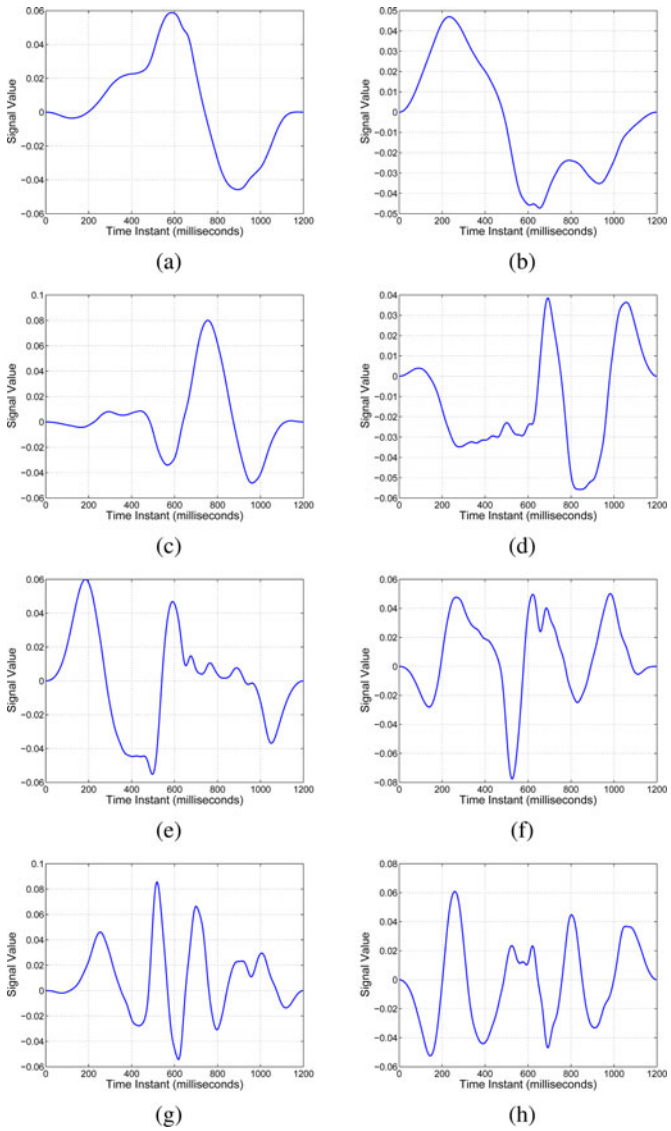

Fig. 3. Ffirst eight principal components generated from the set of training samples.

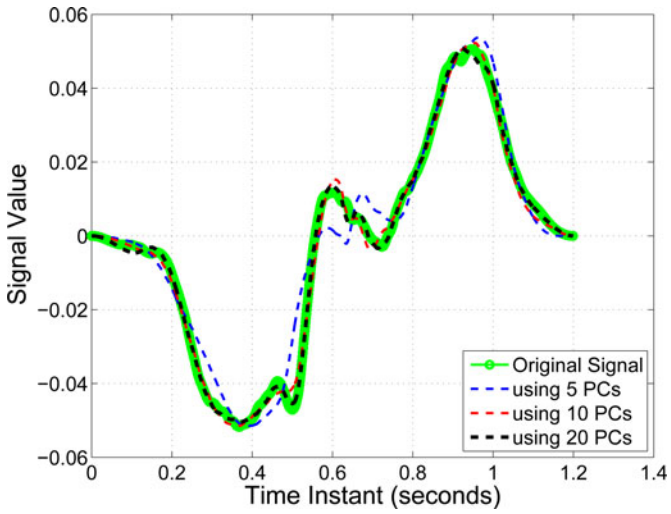

Fig. 4. Example of an RFII recording of one heartbeat duration and it's reconstruction using 5, 10, and 20 principal components (PCs).

TABLE I
SIGNAL RECONSTRUCTION ERROR USING VARYING NUMBER OF COEFFICIENTS IN THE SUBSPACES DISCUSSED

No. of bases	PCA	ICA	Random	KSVD
20	4.03×10^{-5}	2.47×10^{-4}	1.19×10^{0}	2.68×10^{-6}
10	4.13×10^{-5}	1.72×10^{-4}	9.12×10^{-1}	6.75×10^{-6}
5	7.44×10^{-5}	8.52×10^{-4}	7.58×10^{-1}	1.45×10^{-5}

represented as

$$\mathbf{x_i} = \sum_{k=1}^{K} a_k \mathbf{s}_k. \tag{1}$$

Using vector-matrix notation, the mixing model can be represented as

$$\mathbf{x} = \mathbf{A}\mathbf{s} \tag{2}$$

where $\mathbf{s}$ is a $K \times 1$ column vector of unknown source signals at a particular time instant during the beat cycle and A is the mixing matrix (model). Estimating the independent components (ICs) involves solving the following

$$\mathbf{s} = \mathbf{A}^{-1}\mathbf{x} \tag{3}$$

To determine the ICs, there are several approaches that have been documented in literature such as the classical non-gaussianity based approach, using negentropy or using maximum likelihood estimation. Hyvarinen *et al.* in [14] present a good description of all these classical methods. We adopt the approach described by Hyvarinen *et al.* in [15] and use their FastICA implementation. In order to build this sub-space, as mentioned in Section III-A, we use the beats extracted from recordings in our training set. In our work, the determined $\mathbf{s}_k$ are taken to be basis functions and the projection coefficients on the bases are the a_k. Before using the FastICA implementation the data is centered by subtracting the sample mean and whitened, so that the individual components are uncorrelated.

In the case of ICA, as against in the case of PCA, there is no deterministic way to know which of the ICs represent maximum variation in data and hence we cannot say which subset of ICs are required for reconstruction of the signal. ICs determined from the dataset are shown in Fig. 5. Examples of reconstruction using different numbers of ICs are shown in Fig. 6. From this figure, we see that unlike PCA, we cannot use simply a smaller subset of bases for signal reconstruction. The corresponding reconstruction errors are reported in Table I.

C. Random Projection

The previous subspace modeling techniques discussed in this paper are data-driven approaches, in which the subspace is built based on properties of a set of training data. Next, we describe a nondata-driven approach which has been studied in the literature as a versatile method for dimensionality reduction—RP. RP is the technique of projecting a set of data samples from a high-dimensional space to a randomly chosen low-dimensional subspace. Consider an n dimensional data sample (represented as a column vector) $\mathbf{y} = [y_1, y_2, \ldots, y_n]^T$. In order to reduce

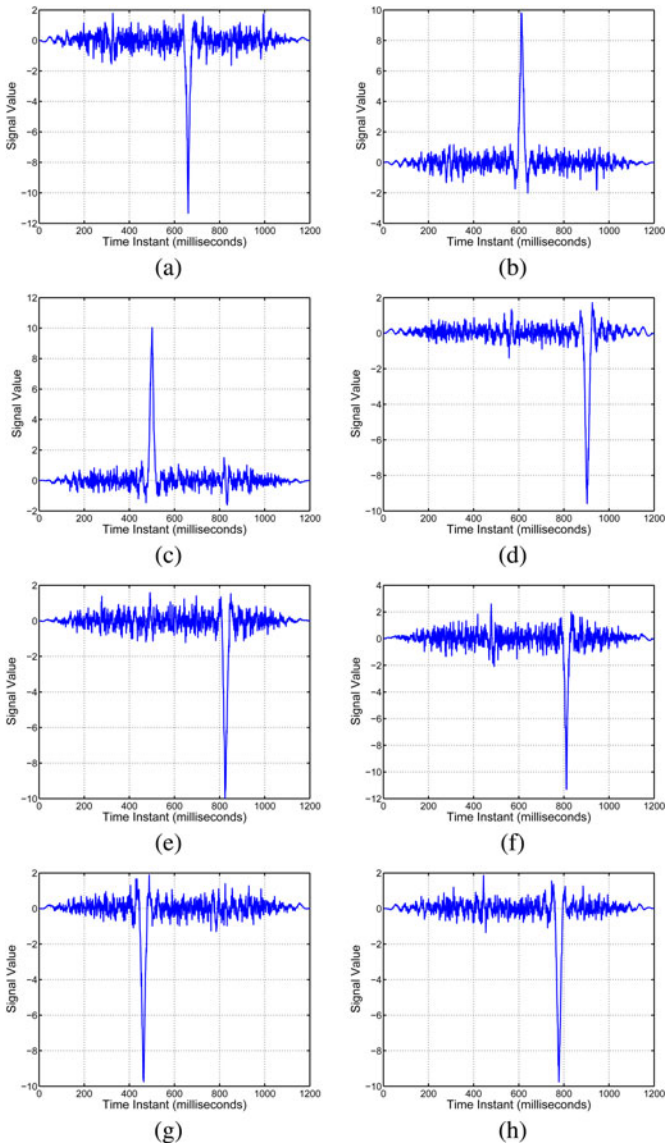

Fig. 5. First eight independent components generated from the set of training samples.

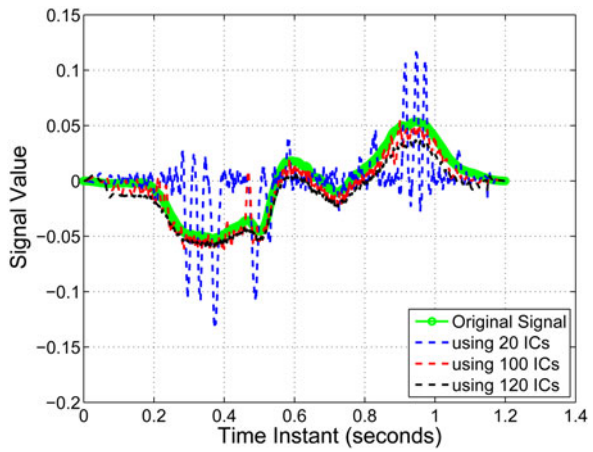

Fig. 6. Example of an RFII recording of one heartbeat duration and it's reconstruction using 20, 100, and 120 independent components.

its dimensionality to a $k < n$, we choose an $n \times k$ matrix $\mathbf{D}$ whose columns are orthogonal unit vectors. $\mathbf{D}$ can be generated by choosing its entries from a normal distribution and orthonormalizing the columns using Gram–Schmidt process. Then, the projected vector is given by (see review by Vempala [23])

$$\mathbf{v} = \frac{n}{\sqrt{k}}\mathbf{D}^T\mathbf{y}. \tag{4}$$

If this is the case, then from the lemma presented and proved by Johnson and Lindenstrauss in [17], the distances between data points in the reduced dimensional subspace is approximately preserved. This lemma is stated here without proof.

Lemma III.1: For any ϵ such that $\frac{1}{2} > \epsilon > 0$ and any set of points $S \in \mathbb{R}^n$, with $|S| = m$, upon projection to a uniform random k-dimensional subspace where $k \geq \frac{9 \ln m}{\epsilon^2 - \frac{2}{3}\epsilon^3} + 1$ the following property holds with probability at least $\frac{1}{2}$, for every pair $y, y' \in S$,

$$(1-\epsilon)\|y - y'\|^2 \leq \|f(y) - f(y')\|^2 \leq (1+\epsilon)\|y - y'\|^2$$

where $f(y), f(y')$ are the projections of y, y'

The result of using this lemma is that inspite of the reduction in the number of dimensions, the original distance between the samples is approximately preserved and hence the classification performance will remain similar to that exhibited in the original space (for classifiers based on the Euclidean distance measures, which is what we use). In our application for the sake of lower number of dimensions, we choose an $\epsilon = 0.499$. In our training database, we have 27 users each with 80 beat samples. Hence, the number of samples $m = 2160$ and we can use the above lemma to determine $k \geq 416$. We choose $k = 420$ in our experiments. Identification rates in this subspace are presented in Section IV. In Fig. 7, we show examples of random bases, and in Fig. 8 we show reconstruction results after projection onto the random subspace. As is clear, this subspace is not optimal for preserving the variation in data and hence exhibits greater reconstruction error (Table I compares the reconstruction error over our test dataset for all the modeling techniques discussed in this paper). In the next section, we describe how we modify this random bases set for the purpose of reducing reconstruction error. The RP method reports very high values of identification rates. The identification rates reported are based on projection onto these 400 bases as well as onto a subset of these 400 bases, for sake of comparison with the other methods in this paper.

D. K-SVD-Based Dictionary Learning

Researchers in signal and image processing have worked on designing overcomplete dictionaries for sparse representation of signals for a variety of purposes. This includes image denoising [11], compression [7], [8], classification [25], [26] amongst others. It was found that overcomplete basis functions have advantages such as flexibility, robustness to noise, and reduced number of basis required to represent a function.

In our study, we use the K-SVD algorithm proposed by Aharon *et al.* [1] in order to learn an overcomplete dictionary starting from a set of random bases as in Section III-C, to minimize reconstruction error of a set of input samples (i.e.,

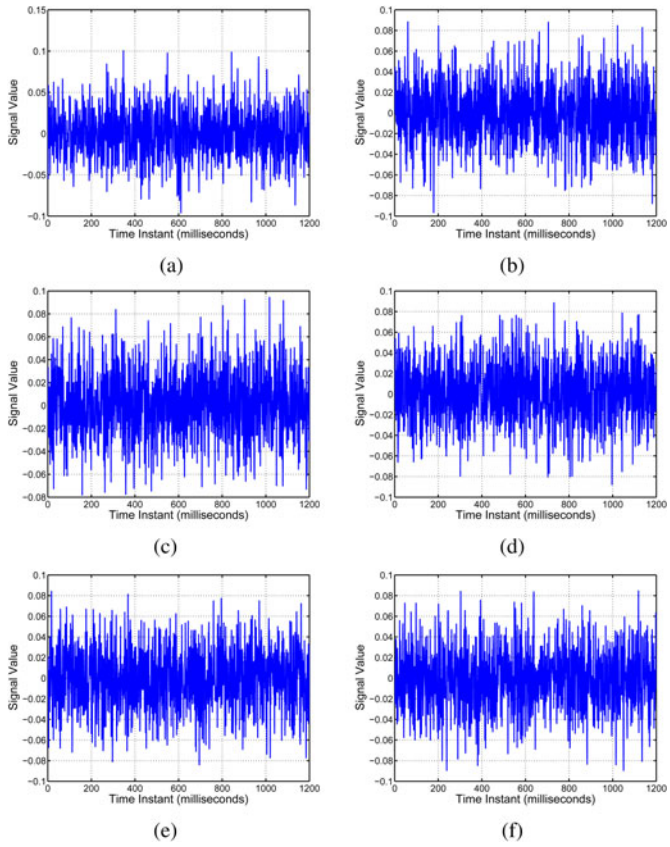

Fig. 7. Six random bases generated for the random projection method discussed here.

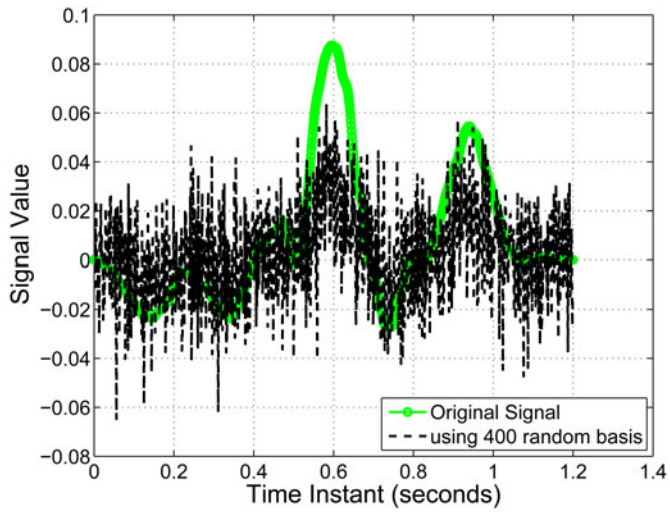

Fig. 8. Example of an RFII recording of one heartbeat duration and its reconstruction using projection onto our set of 400 random bases.

our training samples from each class in our database). Their algorithm tunes the dictionary as well as the corresponding coefficient set so that, for a set of input data, we achieve the best dictionary and sparse coefficient set in order to minimize an l_2 error.

Once the dictionary is determined, given any test sample from a class in the database, we determine the corresponding sparse representation in the dictionary. Next, we pick the class to which the sample belongs by two independent means. These are reported as two experiments in the next section.

1) Pick the class corresponding to that sample in the training data, which has a similar sparse coefficient set.
2) Reconstruct the test sample based on the sparse coefficient set and perform a nearest neighbor classification using all the reconstructed training samples.

The way we use the KSVD algorithm is explained next. First, as explained in the previous section, we generate a set of random orthonormal vectors. The elements of each vector are drawn from a uniform distribution. This will serve as a "seed" dictionary for initialization. The dictionary atoms are the columns of the dictionary matrix $\mathbf{D}$. Consider the set of training data (in other words, our gallery dataset) $\mathbf{Y} = \{\mathbf{y}_1, \mathbf{y}_2, \ldots, \mathbf{y}_N\}$. Given $\mathbf{D}$ and the set of training data $\mathbf{Y}$, we can estimate an initial set of sparse coefficients $\mathbf{X} = \{\mathbf{x}_1, \mathbf{x}_2, \ldots, \mathbf{x}_N\}$ that minimizes an F-norm objective function with a sparsity constraint

$$\begin{aligned} \underset{\mathbf{X}}{\text{argmin}} \quad & ||\mathbf{Y} - \mathbf{D}\mathbf{X}||_F^2 \\ \text{s.t.} \quad & ||\mathbf{X}||_1 < \alpha \end{aligned} \tag{5}$$

where α is the sparsity constraint. Ideally, the sparsity is ensured by using an l_0-norm $||\mathbf{X}||_0 < \alpha$. However, it is well known that this problem is intractable. A more practical solution is to relax the l_0-norm constraint and use an l_1-norm constraint. Recent works have addressed the stability of this relaxation and its ability to yield the exact solution estimated by an l_0-norm.

As an initial step, an orthogonal matching pursuit (OMP) approach is used with the sparsity constraint in order to estimate $\mathbf{X}$, such that the objective function in (5) is minimized. Following this, every dictionary atom is updated along with the the corresponding coefficients in $\mathbf{X}$ using singular value decomposition. Allowing a change in coefficient values while updating the dictionary atoms accelerates convergence, since atom updates in subsequent iterations will be based on "better" coefficients. A detailed description of dictionary update can be found in the seminal work by Aharon *et al.* in [1]. Here, we provide only a very brief overview of the algorithm as used in this study.

1) We start with the initial sparse set of coefficients $\mathbf{X}$ estimated by using OMP.
2) In order to update dictionary atom $\mathbf{d}_i$, consider the dictionary $\mathbf{D}$ and the coefficient set $\mathbf{X}$ to be split up as follows

$$\begin{aligned} \mathbf{D} &= [\mathbf{D}_1 \mathbf{d}_i \mathbf{D}_2] \\ \mathbf{X}^T &= [\mathbf{R}_1 \mathbf{r}_i \mathbf{R}_2]\,. \end{aligned} \tag{6}$$

3) The objective in (5) can be rewritten as follows:

$$\begin{aligned} ||\mathbf{Y} - \mathbf{D}\mathbf{X}||_F^2 &= ||\mathbf{E} - \mathbf{d}_i \mathbf{r}_i||_F^2 \\ \text{where } \mathbf{E} &= \mathbf{Y} - \mathbf{D}_1 \mathbf{R}_1^T - \mathbf{D}_2 \mathbf{R}_2^T\,. \end{aligned} \tag{7}$$

4) However, due to the sparsity constraint in the OMP stage, there are many zeros entries in the vector $\mathbf{r}_i$. Let $\tilde{\mathbf{r}}_i$ be formed by the subset of nonzeros entries in $\mathbf{r}_i$. As a result of this, only the corresponding subset of columns in $\mathbf{E}$ will contribute to the norm in (7). Let this modified $\mathbf{E}$ be

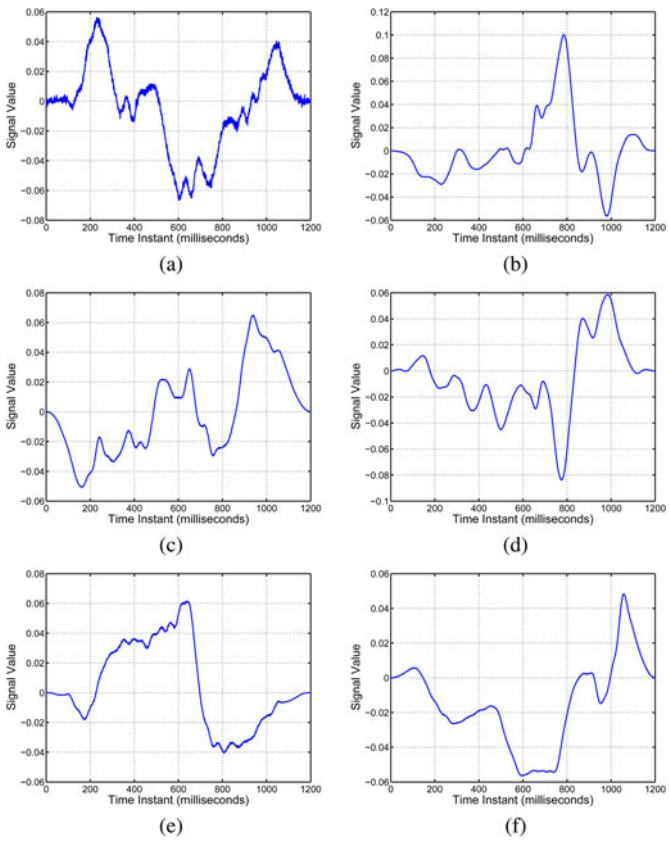

Fig. 9. Six dictionary elements from the KSVD-based dictionary building using our training dataset.

represented as $\tilde{\mathbf{E}}$. Then,

$$||\mathbf{Y} - \mathbf{DX}||_F^2 \propto ||\tilde{\mathbf{E}} - \mathbf{d}_i\tilde{\mathbf{r}}_i||_F^2. \tag{8}$$

The $\mathbf{d}_i$ and $\tilde{\mathbf{r}}_i$ pair can be updated using a rank-1 approximation of $\tilde{\mathbf{E}}$ obtained by performing an SVD factorization $\tilde{\mathbf{E}} = \mathbf{U}\boldsymbol{\Delta}\mathbf{V}^T$. $\mathbf{d}_i$ is set as the first column of $\mathbf{U}$ (i.e., corresponding to the largest singular value) and $\tilde{\mathbf{r}}_i$ is set as the product of the first (largest) singular value in Δ and the first column of $\mathbf{V}$.

5) Steps 2–4 are repeated for all $\mathbf{d}_i$ till the function in (8) falls below a preset threshold value.

Once the KSVD algorithm has converged, the resultant dictionary is used during the matching stage. During the testing stage, we use OMP to solve (5), with test samples occupying the data matrix $\mathbf{Y}$. Identification rates as well as genuine and imposter match scores are shown in Section IV based on the classification methods mentioned. Example bases using this method are shown in Fig. 9 and examples of signal reconstruction are shown in Fig. 10. From Figs. 4, 6, 8, and 10, we see that the KSVD bases as well as PCA bases show minimal reconstruction error. This is supported by theory as well, since the former has a dictionary optimized to minimize the reconstruction error, while the latter preserves the variance of data in its bases. The average mean squared error across the entire database, between the reconstructed signal and the original signal is reported in Table I.

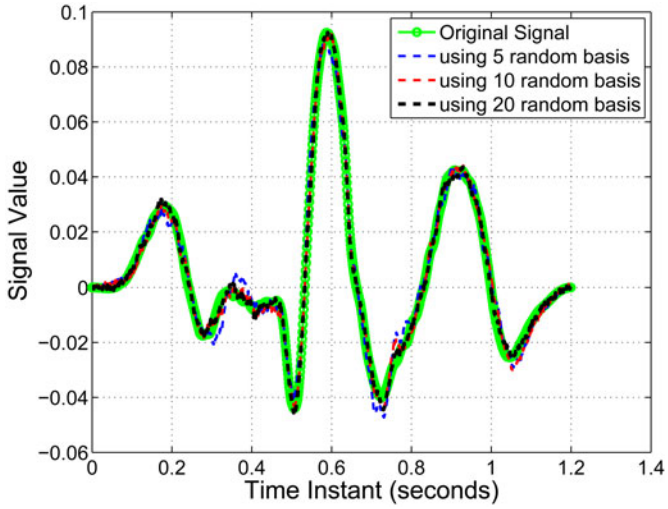

Fig. 10. Example of an RFII recording of one heartbeat duration and its reconstruction using projections onto different numbers of bases using the KSVD algorithm.

IV. Experiments and Results

In this section, we report the results of recognition experiments performed using the various subspace modeling techniques outlined in Section III. We also report the signal reconstruction errors in Table I. This is the average mean squared error across the database between the reconstructed signals and original signals. All the results reported are average results calculated over multiple experiment runs. The results are reported on two sets of data.

1) The first dataset has a total of 27 users with three recordings each. Each of these recordings was captured during a single capture "session." For data acquisition during a session, the subject wore an over the shoulder harness, the operator placed the device in the harness and adjusted the straps so that the device is over the lower sternum of the subject. Once positioned, the operator started recording data for approximately 90 s. The sampling frequency of the device is 1000 Hz. After each recording, the device and harness were taken off. The process was repeated for the subsequent two recordings. Acquisition of each data recording was spaced 15–30 min apart. One recording for every user is taken as the gallery (training) set and the remaining two are taken as the probe (testing) set. From each recording, 80 beat samples are extracted (example of a recording and beat samples extracted are shown in Fig. 1).
2) The second dataset has a total of 21 users, with six recordings each. The difference here is that the recordings of a subject were captured in three separate capture sessions on three different days (two recordings per session). The aim here is to investigate the ability to extract consistent biometric features from recordings made over a longer span of time. The days were spaced apart randomly (based on the subject's schedule)—in some cases it was two days apart and in some cases weeks. Two recordings were made per day per subject in this dataset. The procedure to acquire the signal was the same as described previously.

In this section, we report classification results on both the aforementioned datasets separately. For any given classification method, we report the average result over multiple experiment runs, as mentioned earlier. An experiment run is as follows:

1) Randomly choose a subset of the dataset to be the training set and the remainder to be the testing set. As mentioned earlier, in the single session database, we have 27 subjects who participated in the data acquistion stage and there are three recordings for each subject. In the beginning of an experiment run, for each subject we randomly select one of the recordings as the training recording for that subject and the remainder as the test recordings. For the three session database, two recordings, each from a different session are used in the training set and both recordings from the third session are used as the testing set.
2) The subspace is built using the techniques outlined in Section III, using the training data.
3) Both the testing and training samples are projected onto this subspace and the coefficients are used as the feature vectors. In the case of the K-SVD experiment, we use OMP to determine a sparse coefficient set for the data sample.
4) A k Nearest Neighbor (kNN)-based classifier is used to classify each test sample based on its k nearest training neighbors. We show identification results as well as the distribution of scores in this section.
5) There are two types of results reported in this section—one where we do single beat classification and one where we do classification of an entire recording. In the former case, we extract from every RFII recording, signal data corresponding to every heartbeat duration and classify each of these "beats" separately. In the latter case, we classify all beats from a recording and classify the recording based on a majority vote from amongst the classification labels attached to the constituent beats. Both these sets of experiments are represented in Fig. 11.

The experiments for the three session database classify entire recordings and not individual beats, because as shown in the next subsection, classifying entire recordings is a much more reliable method of identification. Further details of the experiments using three session data are given in Section IV-B.

A. Results on Single Session Data

Table II shows the identification rates obtained when using the kNN classifier to classify the set of recordings in our test dataset. Table III reports the corresponding rates when the individual beats in all these recordings are treated as separate samples and classified. We see that classifying a user using all the beats in his/her recording reports better identification accuracies than classifying a user based on the signal from one heartbeat duration. We also note from the results that the RP method as well as the KSVD-based method report higher rates compared to the rest. In the case of the KSVD based method, as mentioned earlier, we performed an additional experiment where we compared samples based solely on their sparse coefficient set. The corresponding identification rates when using 20, 10, and 5 bases are 66.7%, 53.7%, and 55.6%, which are lesser than the rates observed during the signal reconstruction based KSVD experiment.

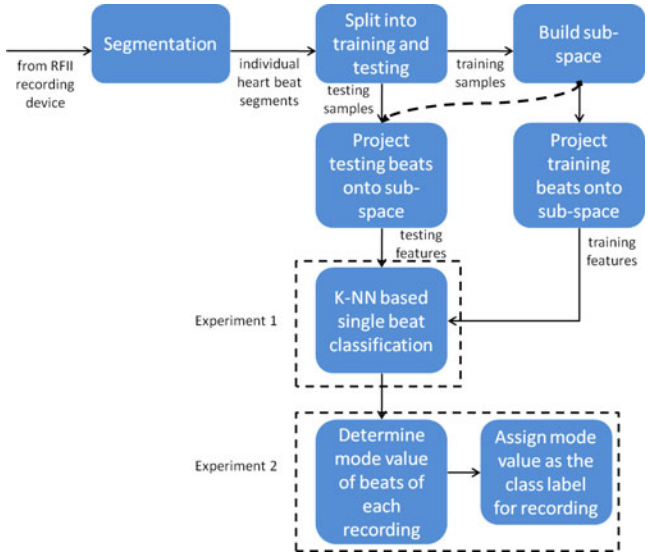

Fig. 11. Illustration of our experiment setup. As shown we report two sets of results—one corresponding to single beat classfication where we are agnostic to the recording and the other corresponding to classification of an entire recording composed of multiple beats. Corresponding results are shown in Tables II and III.

TABLE II
IDENTIFICATION RATES OVER THE TEST DATA-SET OF RFII RECORDINGS

No. of bases	PCA	ICA	RP	KSVD
20	88.9	90.3	92.9	91.9
10	87.9	90.6	89.8	91.9
5	79.3	82.6	85.6	90.4

TABLE III
IDENTIFICATION RATES OVER THE TEST DATA-SET OF BEATS FROM RFII RECORDINGS

No. of bases	PCA	ICA	RP	KSVD
20	74.8	77.3	76.5	79.2
10	73.0	71.3	73.1	78.2
5	61.7	60.6	64.2	77.6

In the case of the RP method, when our test dataset was projected onto 400 random bases, the observed identification rate was 90.7%. The table reports identification rates using a subset of these bases, in order to compare the performance with other methods. Inspite of the reduced number of bases, the results are seen to be similar. The reason for this may be that, even though there are 2160 beat samples, all the beats belonging to a particular user are very similar to each other. Hence, the effective number of beats (m in the lemma) is much lesser. Therefore, the k value determined will be much lesser than 416.

If the data samples were used, with no subspace projection, in the kNN classification framework, then the observed identification rate is 90.7%—this value is very close to the values shown in the tabulated results. Hence, we see that subspace-based classification carries merit due the dual advantages of reduced dimension and high classification accuracies.

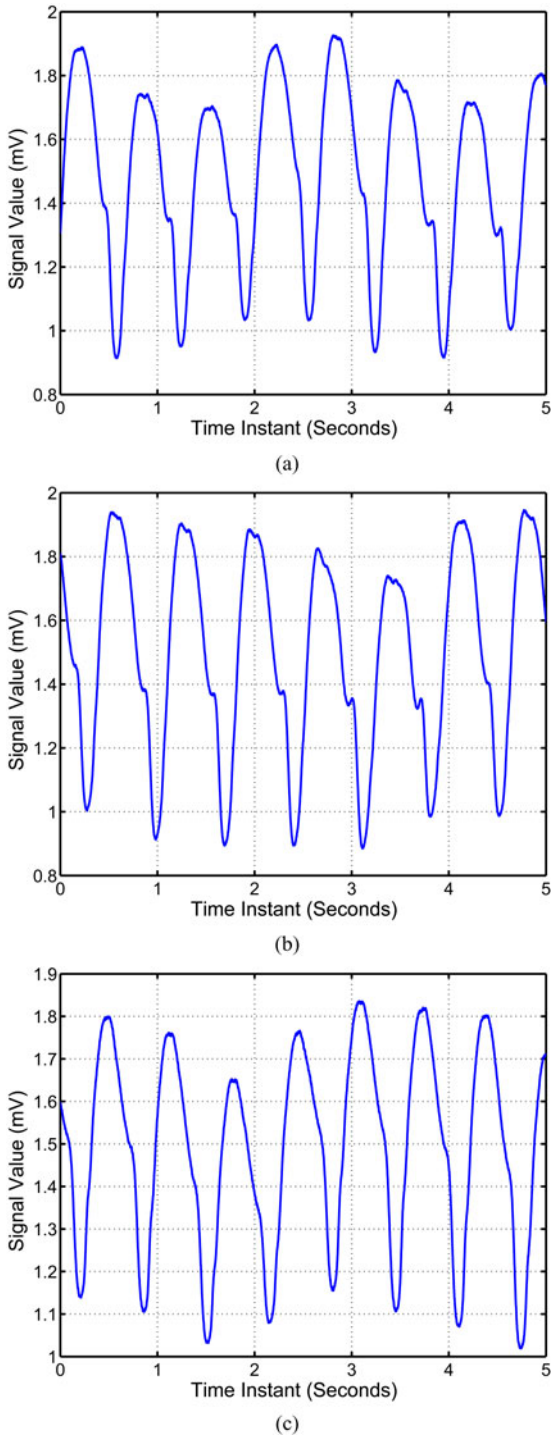

Fig. 12. (a)–(c) show 5 s of three recordings from a single capture session of a subject.

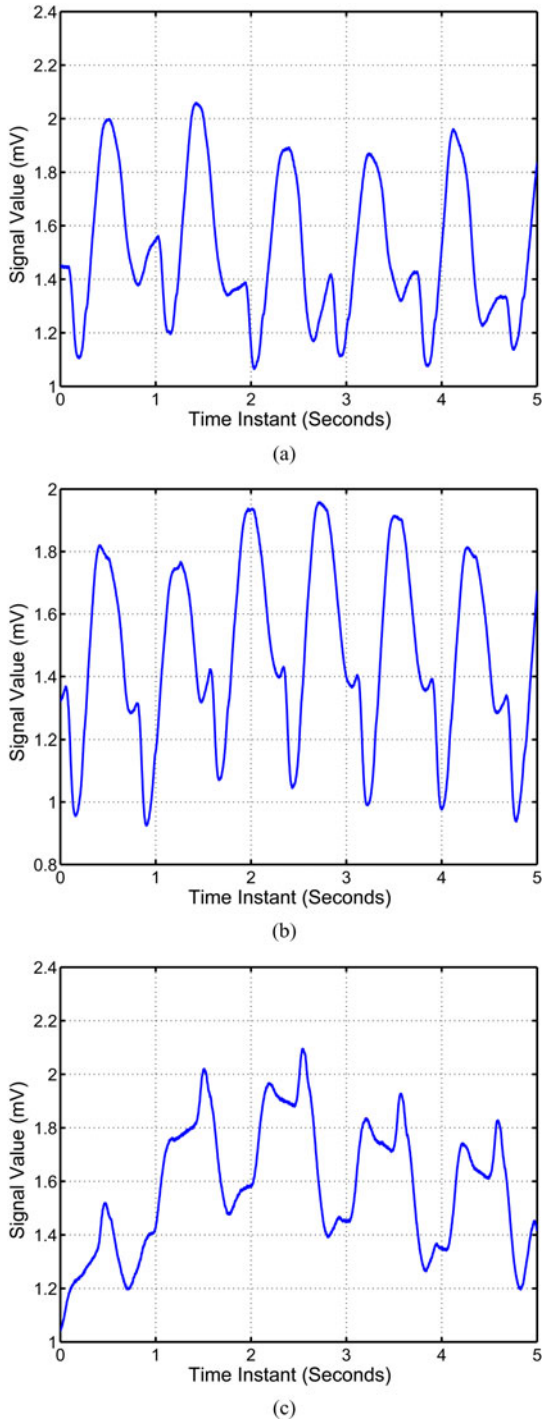

Fig. 13. (a)–(c) shows 5 s of three recordings from three different capture sessions of a subject. Visually, the recordings look less similar than the case depicted in Fig. 12.

B. Results on Three Session Data

In this section, we report the results on the second database, which has recordings from three separate data capture sessions (each session on a different day). The examples of three recordings from the same session for a subject is shown in Fig. 12. The examples of three recordings from the same subject from three different days are shown in Fig. 13. On inspecting the signals, we see that the recordings can appear significantly different on different days, which presents an additional challenge. Simply reducing their dimension using the methods described and using a k-NN classifier does not suffice. In these experiments, two recordings—one from first session and one from the second are used during the training stage, while both the recordings from the third session are used during the testing stage.

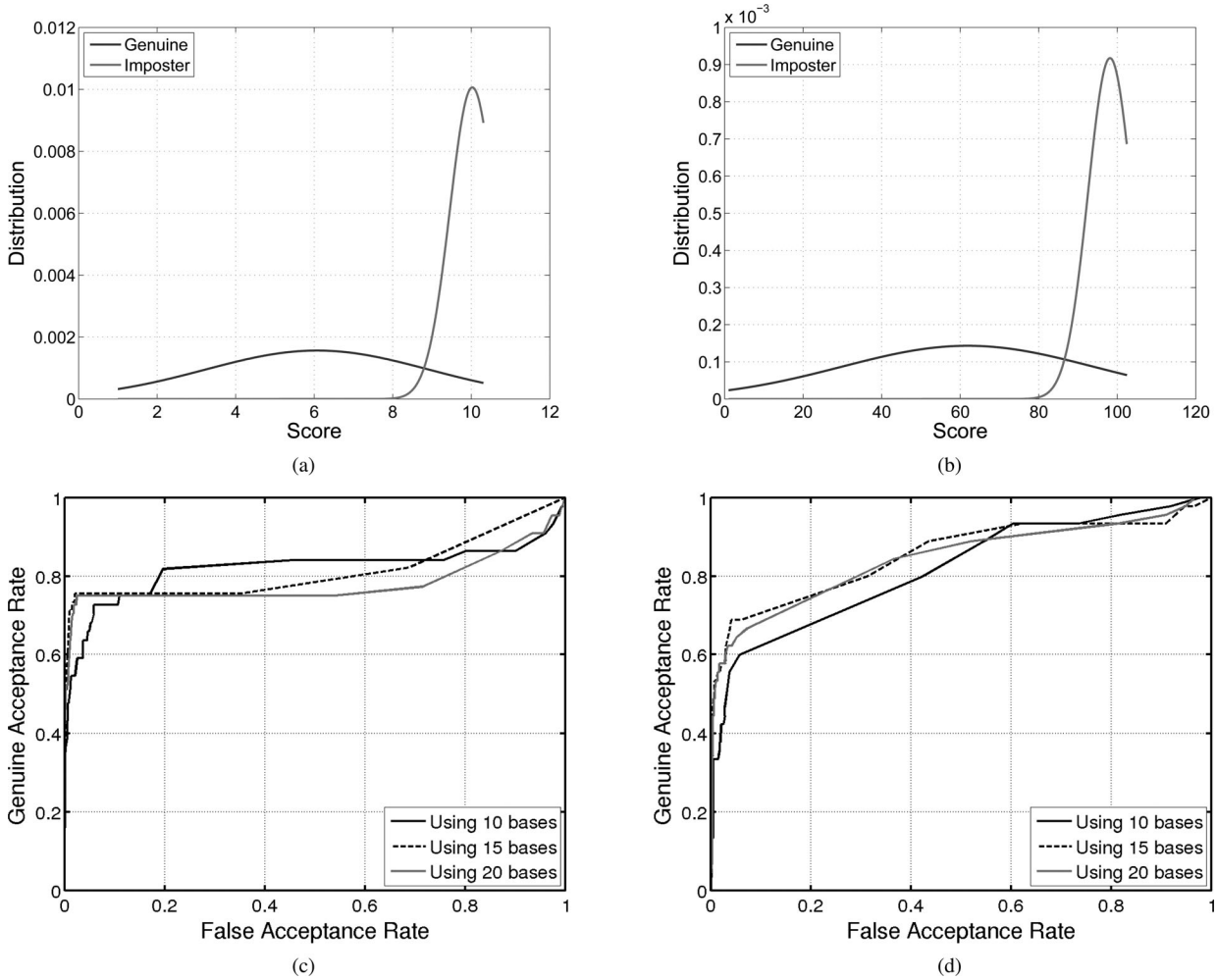

Fig. 14. Genuine and imposter score distributions when classifying low dimensional data in an LDA subspace using (a) a k-NN classifier and (b) SVM models. The corresponding fisher ratios are 1.8481 and 1.2390. The corresponding ROC curves are shown in (c) and (d).

For the purpose of classification, in addition to the k-NN classifier, we also built an SVM model for each class' beats, using the training data. Features for this SVM model are obtained by first using subspace modeling based on PCA and RP described earlier, in order to reduce the dimensionality. The reduced dimension training beats are then used to build a subspace with maximal separation between classes, using a conventional linear discriminant analysis (LDA) approach (a description can be found in [10]). The coefficients of the signal in this LDA subspace are then used as features to build class specific SVM models. For the purpose of this papere, a linear SVM model is built for each class.

During the testing phase, given the test recordings from the third session, the dimension of the extracted beats is first reduced using PCA or RP, following which they are projected onto the LDA subspace to obtain the testing features. We then compare these features against every class' SVM model and note the distance from the SVM hyperplane. By thresholding this distance, we either accept a test sample as belonging to a class or not. Empirically, the normalized distance threshold used by us is 0.7. Any test beat sample at a distance greater than 0.7 from the SVM hyperplane is considered to be a member of that class; otherwise, it belongs to the imposter set. An entire recording is then classified by taking a majority vote of the labels assigned to each beat.

TABLE IV
IDENTIFICATION RATES FOR THE THREE SESSION DATABASE WHEN USING k-NN IN AN LDA SUBSPACE

No. of bases	PCA	RP	PCA + LDA	RP + LDA
20	61.3	48.2	66.4	67.2
15	57.2	47.1	64.5	65.2
10	52.2	38.7	57.8	52.3

Dimensionality reduction is achieved using PCA and random projection.

Using a simple k-NN classifier directly on the beats in the recording (with no subspace projection), the average identification rate seen is close to 47%. Table IV shows the identification rates obtained, using k-NN-based classification in the LDA subspace, when dimensionality was reduced using PCA and using RP. The "number of bases" shown in the table is the bases retained after PCA or RP. Table V shows the corresponding identification rates, when the linear SVM classifier was used on the same data in the LDA space. From the tables, we see that in either case, the identification rates are comparable, with SVM

TABLE V
IDENTIFICATION RATES FOR THE THREE SESSION DATABASE WHEN USING LINEAR SVM IN AN LDA SUBSPACE

No. of bases	PCA + LDA	RP + LDA
20	67.9	63.4
15	65.2	60.1
10	52.2	55.6

Dimensionality reduction is achieved using PCA and random projection.

having a slight advantage in the case of PCA-based reduced dimension data.

Table IV also reports results when k-NN based classification is done on PCA- or RP-based reduced dimension data (first two columns). In all cases, we see that the use of LDA greatly improves the identification rates. Compared to single session data, where the recordings of a subject resemble each other to a certain degree, the three session database reports lower identification rates. However, we have shown that by proper selection of features and classifiers, the identification rates can be improved. Fig. 14 shows the distribution of genuine and imposter scores using both a k-NN classifier and SVM classifier in an LDA subspace (after reducing sample dimension using PCA). The score, in the case of the k-NN classifier, is a function of the probability of belonging to the right class. The probability is estimated based on the number of neighbors belonging to the correct class. The score in the case of the SVM classifier indicates how many beats in the recordings reported a distance greater than the classification threshold. The Fisher ratios corresponding to these distributions are 1.8481 and 1.239. In either case, we see a high variance in the genuine distribution and this may be due to the difference in waveform shape between the training and testing set. However, the imposter score distribution has a much lower variance, which is indicative of a good classifier. The corresponding receiver operating characteristic (ROC) curves are shown in Fig. 14(c) and (d). We see that we are able to achieve high values of genuine accept rates (GAR) at low values of false accept rate. In (c), we get close to 73% GAR at 1% false acceptance rate (FAR) using a standard k-NN classifier in an LDA space.

V. CONCLUSION AND DISCUSSION

In this paper, we have discussed the possibility of using cardio-synchronous waveforms, measured using an RFII device, as a biometric modality. Specifically, the signals we used are waveforms measured from the chest cavity using the RFII device developed by Non-Invasive Medical Technologies. We explored the use of subspace modeling techniques to reduce the dimensionality of the recorded data while preserving its biometric value. We also reported reconstruction errors when reconstructing the higher dimensional signal back from the lower dimensional representations.

We concluded from our experiments that classical methods like PCA, ICA, and RPs perform well when recognition accuracy is the primary metric. Both PCA as well as K-SVD based dictionary building perform very well with respect to this metric. Where these two methods differ is in the reconstruction error experiments. As shown in Table I, the latter method outperforms PCA and reports better reconstruction accuracies and is hence, better suited for the application at hand. For data acquired across days (discussed in Section IV-B), there is a difference in the signal recorded from a given subject. In these cases, KSVD will not be appropriate, since the KSVD algorithm as used in this paper recovers a sparse coefficient set in a dictionary, for minimizing the reconstruction error. The appropriate dictionary will differ, when the signal appears different between sessions. We use an LDA based subspace modeling for these signals and report high identification rates using both a simple k-NN classifier as well as using an SVM model. This is because the use of LDA maximally separates samples of different classes, while reducing the variance of samples within a class to a minimum.

The methods presented in this paper show that discriminative information from an RFII device recording is preserved even in lower dimensional representations. As a result, user templates will be small in size, significantly decreasing database size and database search time for a given number of users. This will prove extremely useful in critical authentication scenarios—such as war zones and highly secure facilities where camera installations are not permitted—by decreasing the response time to any unfortunate incident.

Even though not a strong biometric like the iris or fingerprint, this modality has the advantage of "liveness" detection of the person being tested and the inability to spoof (unlike iris or fingerprint, that may be spoofed, see [24] and [3]). It may be used in tandem with other conventional biometric modalities—face, fingerprint, iris—due to these reasons, to make the final system more resistant to attacks by unwanted individuals. Also, in contrast to ECG and other modalities where electrical impulses are measured, data acquistion is simple with this device. It does not require the use of any electrodes; the data are captured by simply placing the device over an individual's chest. More data are being collected using the NMT RFII device in order to further investigate this technique. Specifically, more data are being collected to study the effects of various hemodynamic states such as sitting, exercising, stress, to name a few, on the acquired signal. From the limited data that we have, from other hemodynamic states, the signal from the same subject looks different across states. Whether this has to do with a posture, or something more intrinsic to the state, is a topic of ongoing research. The ultimate goal will be to extract consistent features across all states, to increase the utility of the device.We feel confident that this line of research will help in developing the RFII-based waveforms into a stronger biometric, which can be used along with, or in place of other state of the art methods in existence today.

REFERENCES

[1] M. Aharon, M. Elad, and A. Bruckstein, "K-SVD: An algorithm for designing overcomplete dictionaries for sparse representation," *IEEE Trans. Signal Process.*, vol. 54, no. 11, pp. 4311–4322, Nov. 2006.
[2] R. Bansal, *Handbook of Engineering Electromagnetics*. New York, NY, USA: Marcel Dekker, 2004.
[3] T. Barsky, A. Tankus, and Y. Yeshurun, "Classification of fingerprint images to real versus spoof," *Int. J. Biometrics*, vol. 4, no. 1, pp. 1–21, Dec. 2012.

[4] C. Bhagavatula, S. Venugopalan, R. Blue, R. Friedman, M. Griofa, M. Savvides, and V. Bhagavatula, "Biometric identification of cardiosynchronous waveforms utilizing person specific continuous and discrete wavelet transform features," in *Proc. 34th Annu. Int. Conf. IEEE Eng. Med. Biol. Soc.*, Aug./Sep. 2012, pp. 4311–4314.

[5] C. Bhagavatula, A. Jaech, M. Savvides, V. Bhagavatula, R. Friedman, R. Blue, and M. O. Griofa, "Automatic segmentation of cardiosynchronous waveforms using cepstral analysis and continuous wavelet transforms," in *Proc. Int. Conf. Image Process.*, 2012, pp. 2045–2048.

[6] M. Bhagavatula, M. Savvides, B. Bhagavatula, R. Friedman, R. Blue, and M. Griofa, "Second degree correlation surface features from optimal trade-off synthetic discriminant function filters for subject identification using radio frequency cardiosynchronous waveforms," in *Proc. IEEE Int. Conf. Image Process.*, Sep./Oct. 2012, pp. 269–272.

[7] O. Bryt and M. Elad, "Improving the k-svd facial image compression using a linear deblocking method," in *Proc. IEEE 25th Convent. Electr. Electron. Eng.*, Dec. 2008, pp. 533–537.

[8] O. Bryt and M. Elad. (2008). Compression of facial images using the k-svd algorithm. *J. Vis. Commun. Imag. Represent.* [Online]. *19(4)*, pp. 270–282, Available: http://www.sciencedirect.com/science/article/pii/S1047320308000254

[9] R. E. Collins, *Foundations for Microwave Engineering*. New York, NY, USA: McGraw-Hill, 1966.

[10] R. O. Duda, P. E. Hart, and D. G. Stork. (2001, Nov.)., 2nd ed. New York, NY, USA: Wiley-Interscience [Online]. Available: http://www.worldcat.org/isbn/0471056693

[11] M. Elad and M. Aharon, "Image denoising via sparse and redundant representations over learned dictionaries," *IEEE Trans. Image Process.*, vol. 15, no. 12, pp. 3736–3745, Dec. 2006.

[12] M. Griofa, R. Blue, R. Friedman, K. Cohen, P. Hamski, A. Pal, R. Rinehart, and T. Merrick, "Radio frequency impedance interrogation monitoring of hemodynamic parameters," in *Proc. Biomed. Sci. Eng. Conf.*, Mar. 2011, pp. 1–4.

[13] M. Griofa, R. Blue, R. Friedman, A. Jaech, M. Bhagavatula, S. Hu, and M. Savvides, "Radio frequency cardiopulmonary waveform for subject identification," in *Proc. 45th Asilomar Conf. Signals Syst. Comput. Rec.*, Nov. 2011, pp. 2152–2156.

[14] A. Hyvrinen, J. Karhunen, and O. Errki, *Independent Component Analysis*. New York, NY, USA: Wiley-Interscience, 1999.

[15] A. Hyvrinen and E. Oja, "Independent component analysis: Algorithms and applications," *Neural Netw.*, vol. 13, pp. 411–430, 2000.

[16] A. Jaech, R. Blue, R. Friedman, M. Griofa, M. Savvides, and B. Bhagavatula, "Classification of cardiosynchronous waveforms by projection to a legendre polynomial sub-space," in *Proc. IEEE 34th Annu. Int. Conf. Eng. Med. Biol. Soc.*, Aug./Sep. 2012, pp. 4307–4310.

[17] W. Johnson and J. Lindenstrauss, "Extensions of lipschitz mappings into a hilbert space," *Contemporary Mathemat.*, vol. 26, no. 189–206, pp. 1–1, 1984.

[18] M. Li and S. Narayanan, "Robust ecg biometrics by fusing temporal and cepstral information," in *Proc. 20th Int. Conf. Patt. Recognit.*, Aug. 2010, pp. 1326–1329.

[19] K. Plataniotis, D. Hatzinakos, and J. Lee, "ECG biometric recognition without fiducial detection," in *Proc. Biometr. Consort. Conf.*, Aug. 2006, pp. 1–6.

[20] C. Polk and E. Postow, *Handbook of Biological Effects of Electromagnetic Fields*. Boca Raton, FL, USA: CRC Press, 1995.

[21] H. Schwan and K. Foster, "Rf-field interactions with biological systems: Electrical properties and biophysical mechanisms," *Proc. IEEE*, vol. 68, no. 1, pp. 104–113, Jan. 1980.

[22] Y. Singh and S. Singh, "Evaluation of electrocardiogram for biometric authentication," *J. Inf. Secur.*, vol. 3, no. 1, pp. 39–48, 2012.

[23] S. S. Vempala, *The Random Projection Method (DIMACS Series in Discrete Mathematics and Theoretical Computer Science)*. Providence, RI, USA: American Mathematical Society, 2004.

[24] S. Venugopalan and M. Savvides, "How to generate spoofed irises from an iris code template," *IEEE Trans. Inf. Forensics Secur.*, vol. 6, no. 2, pp. 385–395, Jun. 2011.

[25] J. Wright, A. Yang, A. Ganesh, S. Sastry, and Y. Ma, "Robust face recognition via sparse representation," *IEEE Trans. Patt. Anal. Mach. Intell.*, vol. 31, no. 2, pp. 210–227, Feb. 2009.

[26] R. Zhang, C. Wang, and B. Xiao, "A strategy of classification via sparse dictionary learned by non-negative k-SVD," in *Proc. IEEE 12th Int. Conf. Comput. Vis. Workshop*, Oct. 2009, pp. 117–122.

Shreyas Venugopalan (S'05) received the Master's degree from the Department of Electrical and Computer Engineering at Carnegie Mellon University, Pittsburgh, PA, USA, in 2009. He is currently working toward the Ph.D. degree at the Cylab Biometrics Center under the guidance of Prof. M. Savvides.

His work includes interdisciplinary research in areas of signal processing, machine learning, and computer vision. His current research interests include design of novel feature extraction and classification schemes for various biometric modalities such as the iris, face, and various biomedical signals. He also works on acquisition of biometric information in unconstrained scenarios as well as in long range surveillance systems.

Marios Savvides (S'03–M'04) is a Research Associate Professor in the Department of Electrical and Computer Engineering, Carnegie Mellon University (CMU), Pittsburgh, PA, USA, and is the Director of CyLab Biometrics Center, CMU. He is one of the four chosen researchers to form the Office of the Director of National Intelligence Center of Academic Excellence in Identity Sciences. His research interests include developing algorithms for robust face and iris recognition as well as in using pattern recognition, machine vision, and computer image understanding for enhancing real-time biometric system performance.

Dr. Savvides is a program committee member on several biometric conferences such as IEEE BTAS, SPIE Biometric Identification, and IEEE AutoID. He has organized and cochaired Robust Biometrics Understanding the Science and Technology (ROBUST 2008) conference. He has authored and coauthored more than 120 journals, conference publications, including several book chapters in the area of biometrics and is an Editor of the Springer's Encyclopedia of Biometrics.

Marc O Griofa received the Graduation degree from University College Dublin, Dublin, Ireland, in 2006, the M.D. degree from University of Limerick, Limerick, Ireland, in 2012, and the Ph.D. degree in biomedical engineering.

He is the Chief Medical and Technology Officer at Noninvasive Medical Technologies Las Vegas, NV, USA, that develops technologies for domestic medicine and defense related applications. He is a Fellow of the Academy of Wilderness Medicine. He is the Principal Investigator for Project CASPER (Cardiac Adapted Sleep Parameters Electrocardiogram Recorder), which was the first Irish experiment to be flown onboard the Space Shuttle and International Space Station.

Dr. Griofa has received the Aerospace Medicine Associations Young Investigators Research Award in 2006 and the Space Medicine award in 2012 for his ongoing research. From 2007 to 2010, he was the part of the spaceflight medical triage team at Kennedy Space Center and worked in conjunction with the aerospace medicine department and biomedical research laboratory due to his research and operational medicine background.

Ken Cohen received the B.Sc. in biology from Seton Hall University, South Orange, NJ, USA, in 1994, and the Ph.D. degree in physiology from the University of Rochestor, Rochester, NY, USA, in 2000.

He is the Lead Physiologist at the physiology and engineering lab, InoMedic Health Applications, Inc., Merritt Island, FL, USA. He has worked on several research projects at the NASA Biomedical Research Laboratory, at the Kennedy space center, and at InoMedic Health Application.